International Journal of Heat and Mass Transfer 182 (2022) 121967

Contents lists available at ScienceDirect

International Journal of Heat and Mass Transfer

journal homepage: www.elsevier.com/locate/hmt

# Enhanced gas-liquid absorption through natural convection studied by neutron imaging

Benjamin Fumey[a,*], Andreas Borgschulte[b], Sascha Stoller[a], Reto Fricker[a], Ralf Knechtle[a], Anders Kaestner[c], Pavel Trtik[c], Luca Baldini[a,d]

[a] Empa, Swiss Federal Laboratories for Materials Science and Technology, Urban Energy Systems Laboratory, Überlandstrasse 129, 8600 Dübendorf, Switzerland
[b] Empa, Swiss Federal Laboratories for Material Science and Technology, Advanced Analytical Technologies Laboratory, Überlandstrasse 129, 8600 Dübendorf, Switzerland
[c] Paul Scherrer Institut, Laboratory for Neutron Scattering and Imaging, Forschungsstrasse 111, 5232 Villigen, Switzerland
[d] Zurich University of Applied Sciences, School of Architecture, Design and Civil Engineering, 8401 Winterthur, Switzerland

ARTICLE INFO

*Article history:*
Received 25 June 2021
Revised 1 September 2021
Accepted 10 September 2021

*Keywords:*
Liquid absorption
Neutron imaging
Long-term heat storage
Concentration-based convection
Heat and mass exchanger design

ABSTRACT

Heat release from absorption storage heat pump by means of absorption of water vapor into aqueous sodium hydroxide is limited by uptake kinetics affecting temperature gain, as well as power- and energy density of the method. Earlier studies pinpoint that natural diffusion alone is not sufficient to reach higher uptake rate, and that the surface to bulk exchange has to be enforced. In this paper, different technical solutions to this problem for the heat storage application are introduced and studied by neutron imaging, enabling visual observation of water vapor uptake and diffusion. The experiments brought to the fore that the buoyancy changes associated with water uptake may be utilized to markedly enhance kinetics. This concept was applied on a vertically installed spiral finned tube operating as heat and mass exchanger for the absorption storage heat pump, also referred to as sorption heat storage. By flooding the space between the spiral fin with absorbent, water absorption into the vertical surface leads to a buoyancy driven movement of the liquid, supplying unspent aqueous NaOH to the vertical surface and exchanging it with the diluted liquid. This is found to increase the rate of absorption markedly. Under realistic heat storage specific operating conditions, a temperature gain of 12.5 K, an active area specific power of 1.28 kW/m$^2$ and an energy density of 243 kWh/m$^3$ in respect to the volume of charged absorbent (greatest volume) is reached. It is proposed that carful design of the spiral finned tube to enhance buoyancy movement will further improve overall sorption heat storage performance.



## 1. Introduction

Liquid absorption heat transformers such as chemical heat pumps and chillers are typical technical gas-liquid absorption processes, providing a temperature shift [1]. Processes are continuous, cycling between absorption and desorption [2]. Liquid absorption heat storage, a form of chemically driven heat pump with absorbent pair storage, follows the same alternating process with objective for heat release at serviceable temperature [3]. However, not in its classical continuous cycling, but with intermittent storage time, bringing forth the need for stored absorption potential, translating to thermal storage capacity [4].

The liquid absorption storage heat pump also referred to as absorption heat storage, is a technology studied and developed for inter-seasonal heat shifting [3]. Systems are charged with surplus solar energy in summer and employed to release heat from a low temperature heat source at serviceable space heating temperature in winter [4]. The concept is a part of a broad range of compact long-term sorption heat pump-based, heat storage technologies including the processes of adsorption on solids as well as absorption on solids and liquids [3].

In the absorption storage heat pump, the absorption heat pump capacity depends on the kinetics of the heat and mass transfer. This counterintuitive behavior stems from the fact that the maximum uptake (release) of the absorbate (in our case here water) by the absorbent (in our case here aqueous NaOH) is a function of the temperature. The higher the temperature, the lower is the total amount of water in aqueous NaOH and vice versa. Heat storage

* Corresponding author at: Empa Materials Science and Technology, Überlandstrasse 129, 8600 Dübendorf, Zürich, Switzerland.
*E-mail address:* benjamin.fumey@empa.ch (B. Fumey).

https://doi.org/10.1016/j.ijheatmasstransfer.2021.121967

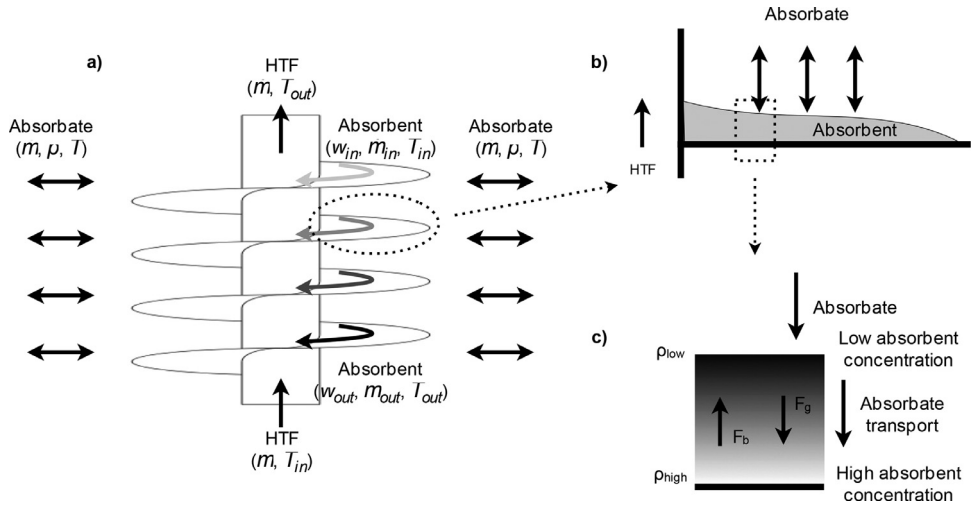


**Fig. 1.** a) Illustration of the spiral finned heat and mass exchanger concept. The HTF flows through the center tube and the liquid absorbent flows on the spiral fin top surface in counter flow to the HTF. Absorbate is exchanged to the absorbate atmosphere, absorbed in discharging and desorbed in charging, illustrated by the changing gray scale of the arrows. b) Illustration of the absorbent film on the spiral fin. c) Illustration of the absorbate uptake in absorption, with the buoyancy force ($F_b$), originating from the gravitational force ($F_g$) and the changing liquid density ($\rho$), in counter direction to the absorbate mass transport. Concentration, and thus solution density increases from top to bottom.

relies on removing heat from a high temperature source by evaporating water, and the reversed process for heat release. However, finite kinetics require an over potential, here a temperature gradient, which translates into an effectively lower (higher) temperature of the absorbent upon heat uptake (release). With this, less adsorbent is released (taken up for heat release) than would be possible in a system with infinitely high kinetics. Research and development focusses thus on the enhancement of the mass transfer being the main kinetic barrier [5].

The technical realization of such absorption heat pump type heat and mass exchangers (HMX) for use in absorption heat storage (see also appendix for further details) may be simplified by assuming a liquid layer of absorbent, here aqueous NaOH, which takes up (releases) water vapor at a given vapor pressure and temperature. For thin liquid layers, the mass transfer is exclusively determined by diffusion of water in the liquid layer; the system is practically "static" [5]. This limits the mass transport drastically. The solution to this problem is apparently simple: the surface to bulk exchange has to be actively enforced. Practical examples include: finned structures to spread the absorbent on the falling film flat plate [6], grooved plate falling film absorbers [7], tube bundle falling film HMX with corrugated mesh guides, and several others. However, all designs depend on high absorbent flow rate, reached by absorbent recirculation, pumping partly discharged absorbent back to the top of the HMX, an action disallowed in the absorption storage heat pump since it leads to severe decline in potential temperature gain.

Our idea of a novel concept of increasing surface-to-bulk mixing is born from a design based on vertically installed spiral finned tube HMXs [8], illustrated in Fig. 1. In this design, the absorbent flows as a thin film, by gravitational force, in spiral formation downwards along the finned tube and the heat transfer fluid (HTF) is pumped in counter flow through the tube. Absorbent channeling along the fin prevents dry inactive areas, long flow distance asserts prolonged exposure time for maximum absorbate uptake and counter flow underwrites good heat exchange. Despite the fact that the absorbent flow is distinctly laminar, we find by carefully designed model experiments that the buoyancy changes induced by the water uptake/release enhance mass transfer. In order to validate the functionality of our novel approach, we utilized high temporal resolution neutron imaging [9] for visualization of the concentration changes and transport of fluids.

To scrutinize the effect of natural convection on the water uptake by aqueous NaOH, we designed three different experiments based on time resolved neutron radiography. The first one analysis the impact of film height and droplet impingement on a horizontal quiescent liquid absorbent film (Section 3.1). The original idea was to follow the surface to bulk mixing enforced by droplet impingement through fin segmentation. However, it became clear that the natural convection had a much bigger impact than the short mixing induced by impingement. To further analyze the buoyancy effect, we designed an experiment, in which the liquid film is put upside down (suspended film / droplet). The contrary behavior is expected and indeed found (Section 3.2). Finally, a model of the finned tube scenario is studied. Here, the natural convection induces a circular flow beneficial for the water uptake rate (Section 3.3). This concept was realized in a single tube model HMX, changing from thin absorbent film flow shown in Fig. 1, to flooded fin flow illustrated in Fig. 7, with good mass transfer rates (Section 3.4).

It is understood that in addition to the gravity force-based buoyancy movement from changing solution density through absorbate uptake or release, effects such as the Gibbs-Marangoni effect may become active, particularly at instances of high concentration and temperature gradient. For example, during initial absorbate uptake on highly concentrated absorbent. Nevertheless, this is not considered in this study, and would require further reflection, particularly in light of the continuously changing surface tension, concentration gradient, temperature gradient and rate of absorption or desorption. Both spatial and temporal resolution of the employed visualization method may not meet the requirements for such analysis.

## 2. Methods section

### 2.1. Neutron imaging

Neutron imaging is an area of study followed since the accessibility of the neutron beam in the 1930s [10]. To date, there are approximately 15 state of the art installations situated at research nuclear reactors and spallation neutron sources, such as the Paul

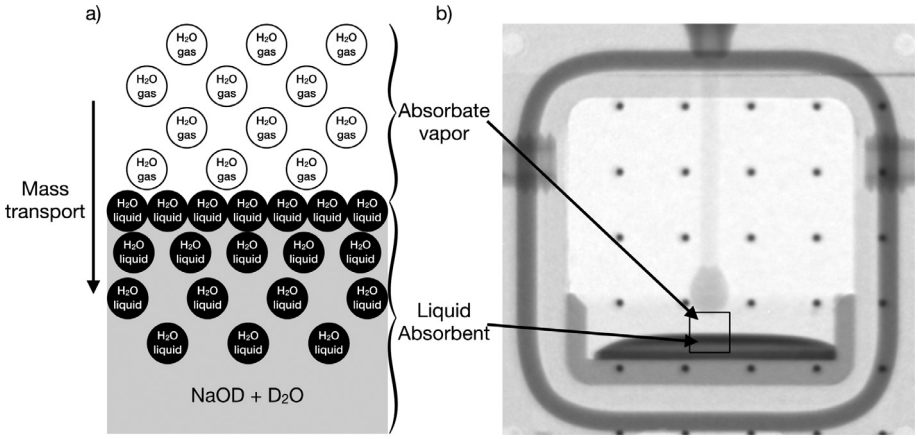


**Fig. 2.** a) Illustration of the visualization of absorbate mass transport. The gaseous absorbate is transparent and becomes visible (black) when liquified on the absorbent surface and transports into the absorbent film. b) Neutron image of the cell showing the chamber vaper volume ($H_2O$ gas), droplet supply and absorbent film (NaOD + $D_2O$). The black dots are for orientation purpose only, originating from an afore-placed aluminum sheet containing highly neutron scattering inlays.

Scherrer Institute (PSI) Swiss Spallation Neutron Source (SINQ) facility, with the Cold Neutrons imaging (ICON) beam line employed in this work [10,11].

Due to its weak interaction with many higher density materials, the neutron is a unique probe in non-destructive investigations of materials and component [12–15]. Hydrogen is one of the most prominent neutron scatterers, providing high sensitivity to water [16]. Furthermore, neutrons are isotope sensitive. Particularly for hydrogen, there is a great contrast difference between the two isotopes $^1H$ and $^2H$ (deuterium) [17], a characteristic exploited in this experiment. Classically, neutrons are attenuated (due to scattering) by the hydrogen in water ($H_2O$) and sodium hydroxide (NaOH) and to a substantially lower degree by sodium (Na) and oxygen (O). In order to improve contrast of absorbent (NaOH + $H_2O$) to absorbate ($H_2O$), the experiment is followed through with isotopically-enriched absorbent solution, thus the hydrogen in the absorbent solution is replaced with deuterium, NaOD and $D_2O$, while the absorbate vapor is kept as conventional water ($H_2O$). In this way, the neutron beam provides a hydrogen sensitive radiographic image. Fig. 2a illustrates the image contrast; whereby gaseous $H_2O$ is non-visible. Although it contains hydrogen in its primary isotope state, the low material density renders it transparency. The liquid absorbent, containing hydrogen in its second isotopic state, is also transparent. Liquified water vapor, absorbed on the liquid absorbent on the other hand, becomes visible as dark areas, areas where the neutrons are scattered and absorbent concentration is reduced. Transport of this liquid water into the absorbent and mixing is made visible by gray scale.

The temporal and spatial resolution of the images are mutually limited by the neutron flux. One is optimized on the expense of the other, both have been refined by digital detection and image processing [18-23]. In this study, exposure times of 0.1 s and 1.0 s with a resolution of 44 µm are applied. The test object is closely positioned to the scintillator screen to reduce the amount of penumbra blurring. Images are referenced in respect to dark current and open beam image.

### 2.2. Test cell

The aluminum test cell shown in Fig. 3a is used. Aluminum is mostly transparent to neutrons and withstands the applied vapor to atmosphere pressure difference. In the cell all gasses apart from water vapor are removed. To prevent absorbent contact, a polytetrafluoroethylene (PTFE) tray is inserted inside the cell. Like the aluminum PTFE is mostly transparent, having a relatively low attenuation coefficient and containing no hydrogen. Samples are placed on a stainless-steel metal sheet on the tray bottom. For sample supply, a thin PTFE tube is inserted from the cell top. The cell is connected to a water ($H_2O$) vapor source, vacuum pump and pressure sensor. Absorbent supply is tubing pump regulated.

Observation of absorption and convection is performed under three varying conditions: increasing film height (thickness), droplet suspension, and fin segment embedment. The study is performed under absorbate atmosphere, with quiescent absorbent, and non-controlled absorption heat release. Tests are performed at 2.33 kPa water vapor pressure, equivalent to 20 °C evaporating temperature and the absorbent concentration is 40wt% NaOD in $D_2O$.

### 2.3. Lab test bench

A test bench was built to examine the flooded spiral finned heat and mass exchanger (HMX). The setup consists of two interconnected chambers (absorber / desorber and evaporator / condenser) of cylindrical shape, 1400 mm high and 100 mm in diameter. Fig. 3b shows the setup. Each chamber contains a single vertically installed spiral finned tube. The heat transport fluid (water on both sides) is pumped upwards through the spiral fin tube, flow regulated by gear pump. The evaporator fin is flooded with water which is recirculated. The absorber is supplied with aqueous NaOH with a concentration of 50wt% to the top of the spiral fin. Discharged absorbent is collected at the bottom of the chamber and released via vacuum lock. The test bench enables realistic testing conditions on a single HMX testing tube. A detailed description of the testing facility can be found in [8].

## 3. Results

### 3.1. Droplet impingement on quiescent liquid absorbent film

The prospect for mass transport enhancement through mixing by droplet impingement on absorbent film is examined. Drops of 2.8 mm diameter are constructed and released at a height of 3.5 mm from the stainless-steel plate. The droplet diameter is not specifically regulated and results from the absorbent viscosity and surface tension in the absorbate atmosphere. The falling height is chosen based on the possible fin spacing in the real setup, and varies dependent on the accumulated film height. Results are shown in Fig. 4, with original images accompanied by contrast enhanced, enlarged records (showing half of the original image with the left border representing the droplet center line), emphasizing

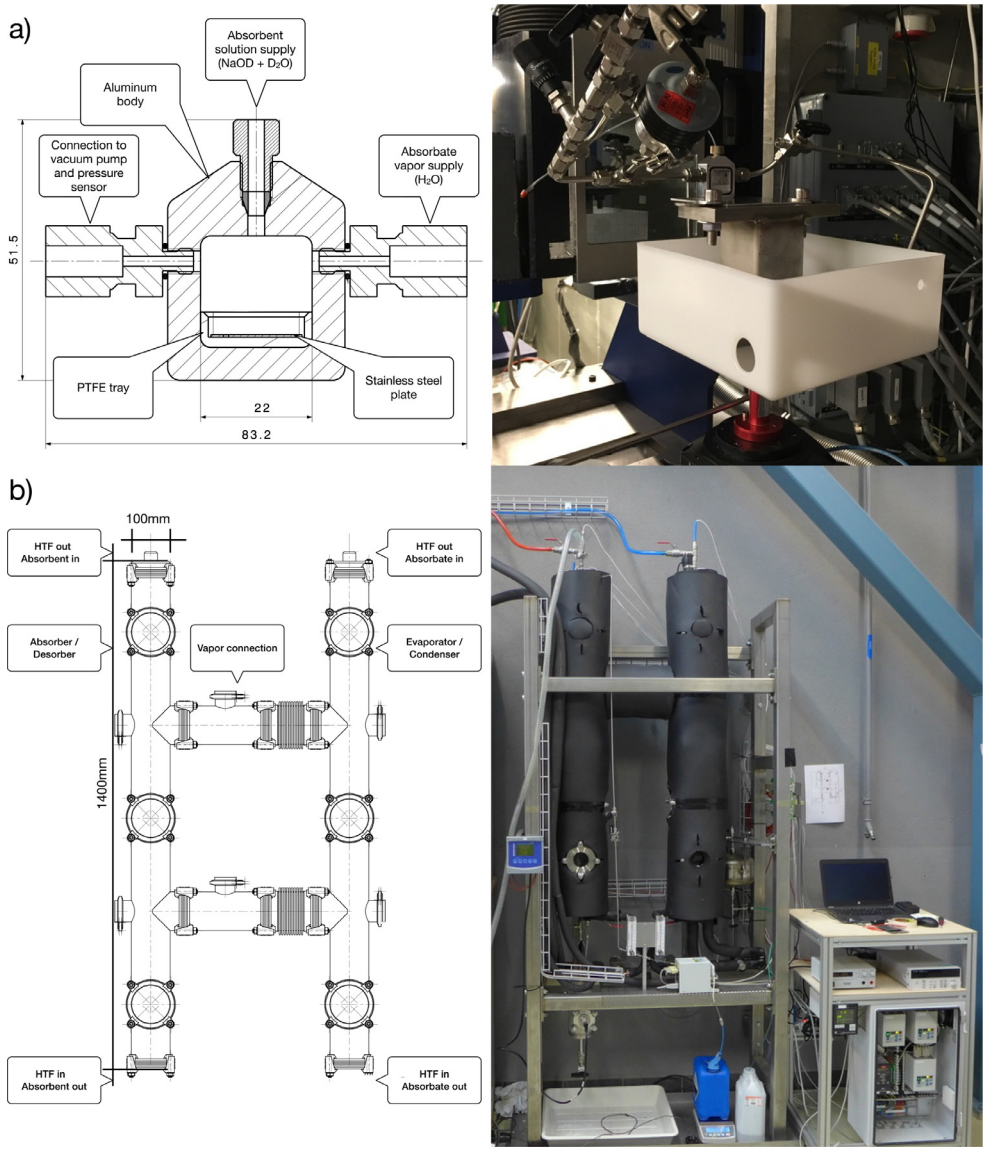


**Fig. 3.** a) Illustration of the test cell on the left and a picture of the test cell installed in the beam line on the right. Measurement values are in millimeters. b) Illustration of the test bench containing the spiral finned tube on the left and a picture of the testing facility on the right.

absorbed water ($H_2O$) vapor diluted absorbent, in black. Red lines are inserted to indicate the steel plate surface and arrows are included in the enhanced image to indicate observed movement of concentrated absorbent (red) and diluted absorbent (blue). Areas of increased water vapor uptake, based on exposure of concentrated absorbent, are indicated with green arrows. White areas within the film contain concentrated absorbent, the film shape can be derived from the original images. Initially, the stainless-steel surface is free of absorbent, except for slight absorbent impregnation, followed by continuous film growth through droplet impingement and deposition. The film height after droplet impingement is indicated in each image as well as the time step from first image. In Fig. 4a, a sequence of images, pre and post droplet impingement is shown with droplets numbered and time step from first image indicated. Fig. 4b shows a follow-up series of images, with one droplet impingement event contained. Succeeding images are shown with time step from first image indicated.

First impingement (D1) accompanies rapid, wide spread and prompt absorbate uptake indicated by the absorbent film appearing all black. The subsequent droplets (D2 to D6) follow a pattern of sideways movement of diluted absorbent, indicated by the arrows, resulting in a more concentrated center of the film with a dilute ring. This behavior can be witnessed by the lighter gray area in the center of the film in Fig. 4a to the left or by the white area in the respective contrast enhanced images. From D4 on, as the film depth increases, this process is accompanied by an under washing of concentrated absorbent forcing diluted absorbent to rise. In the sequence shown in Fig. 4b, this process continues to the extent that the diluted absorbent floats to the top, exposing concentrated absorbent on the sides. The droplet impingement between time 3 s and 4 s produces no visible absorbent mixing. There appears to be a process of surface breakthrough and deposition under the diluted absorbent. The final four images from 14 s to 44 s show a steady increase of the diluted absorbent film thickness (uptake of $H_2O$), with continuous sideways exposure of concentrated absorbent.

### 3.2. Film suspension

Based on the observations presented in Fig. 4, the film suspension test is performed in an attempt to verify natural convection.

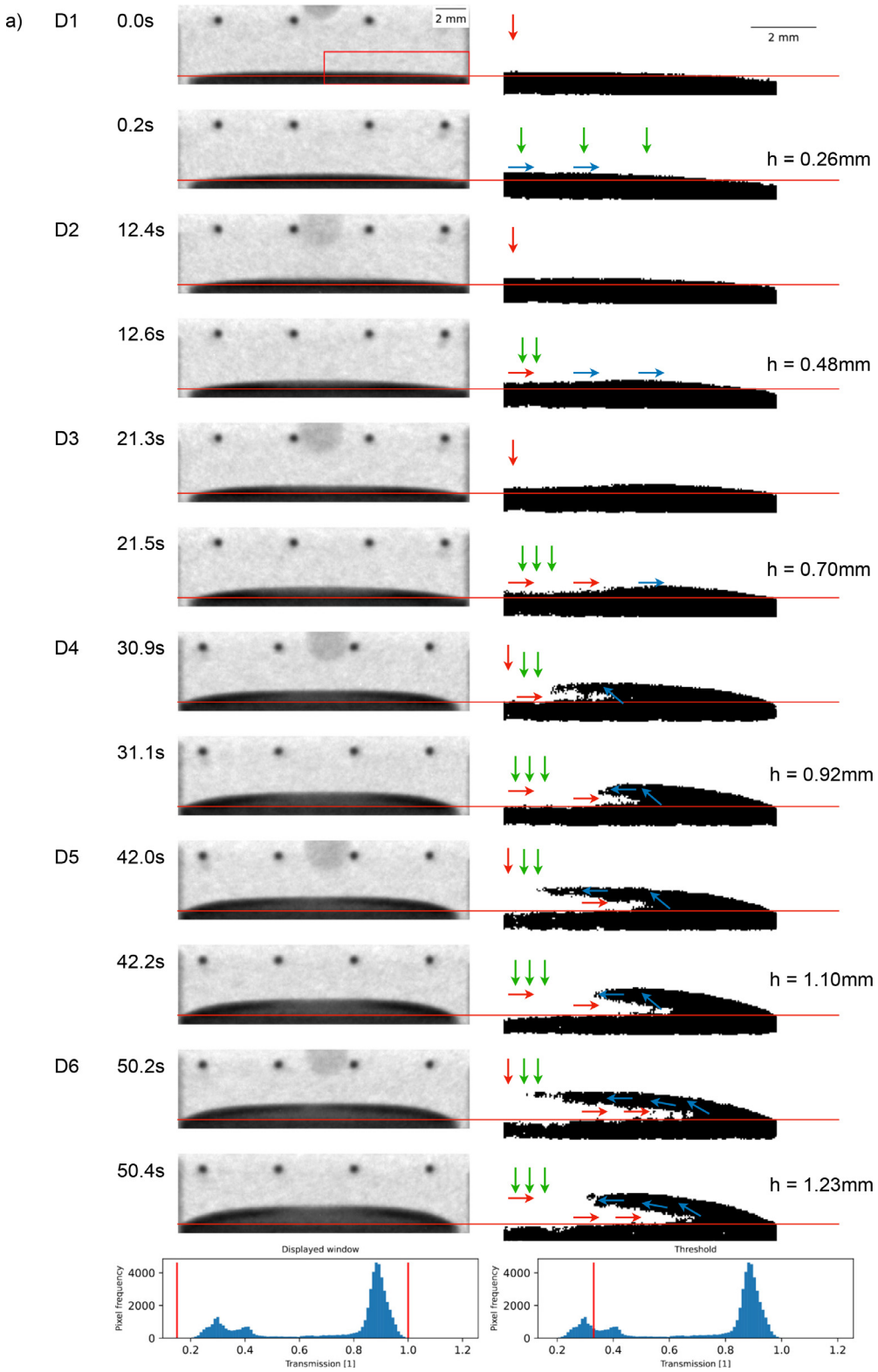


**Fig. 4.** Images showing droplet impingement taken at an image exposure time of 0.1 s (Fig. 4a) and 1 s (Fig. 4b). The horizontal red line indicates the interface between stainless steel plate and absorbent. Dark areas above the red line are regions of diluted absorbent containing absorbed $H_2O$. Images are accompanied with a thresholded, enlarged version, with white areas in the film containing concentrated absorbent. Observed movement is indicated with red arrows for concentrated absorbent, blue arrows for diluted absorbent and green arrows for areas of expected large absorbate uptake. The four black dots are for orientation purpose only. The red vertical lines in the left pixel frequency diagrams indicate the gray level interval displayed. The line in the right diagrams is the threshold used for the segmentation (For interpretation of the references to color in this figure legend, the reader is referred to the web version of this article).

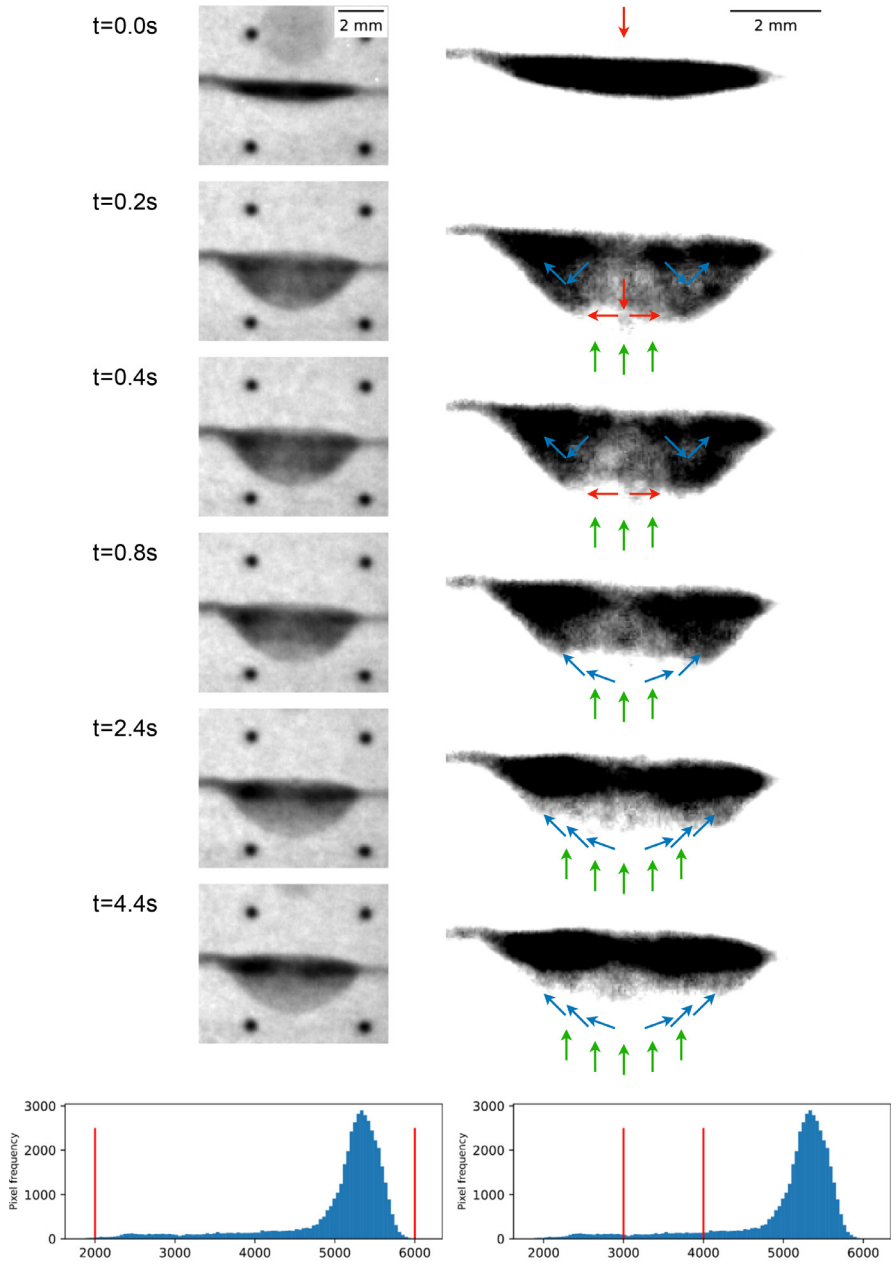


**Fig. 5.** Image sequence of droplet suspension and impingement taken at 0.1 s exposure time. Images are accompanied with a thresholded, enlarged version, with white areas in the droplet containing concentrated absorbent. Observed movement is indicated with red arrows for concentrated absorbent, blue arrows for diluted absorbent and green arrows for areas of expected large absorbate uptake. The four black dots are for orientation purpose only. The red vertical lines in the left pixel frequency diagram indicate the gray level interval displayed. The lines in the right diagram are the threshold area used for the segmentation (For interpretation of the references to color in this figure legend, the reader is referred to the web version of this article).

For this purpose, a stainless-steel wire mesh is installed for absorbent suspension. Droplets from the supply tube fall on and adhere to the mesh and are suspended in the water vapor atmosphere.

Fig. 5 shows the image results, 6 images with noted time step. Again, original and threshold adjusted, enlarged variants are shown. In the commencing image a fresh absorbent droplet drops above a suspended diluted absorbate film. At time 0.2 s, the droplet has fallen, colliding and partly intermixing with the diluted film on the mesh. In the following images, a continuous separation of concentrated and diluted absorbent is observed. Concentrated absorbent sinks to the bottom and diluted absorbent rises to the top, indicated by the respective arrows. Like in the previous setup (Fig. 4), rapid separation occurs. On the contrary, in the droplet suspension case, the concentrated solution is directly exposed with a large surface area to the absorbate from underneath the wire mesh. This increases the concentrated absorbent exposure to absorbate, augmenting power by reducing mass transport hindrance.

### 3.3. Absorbent flooded fin segment

A fin segment, comparable to the spiral finned vertical tube HMX, is installed in the tray. Absorbent is supplied from the supply tube, with droplets impinging on the upper fin and flowing over the fin edge to fill the space between fins.

Fig. 6 shows exemplary images, with time step noted. The process starts with a small deposit of diluted absorbent at the closed

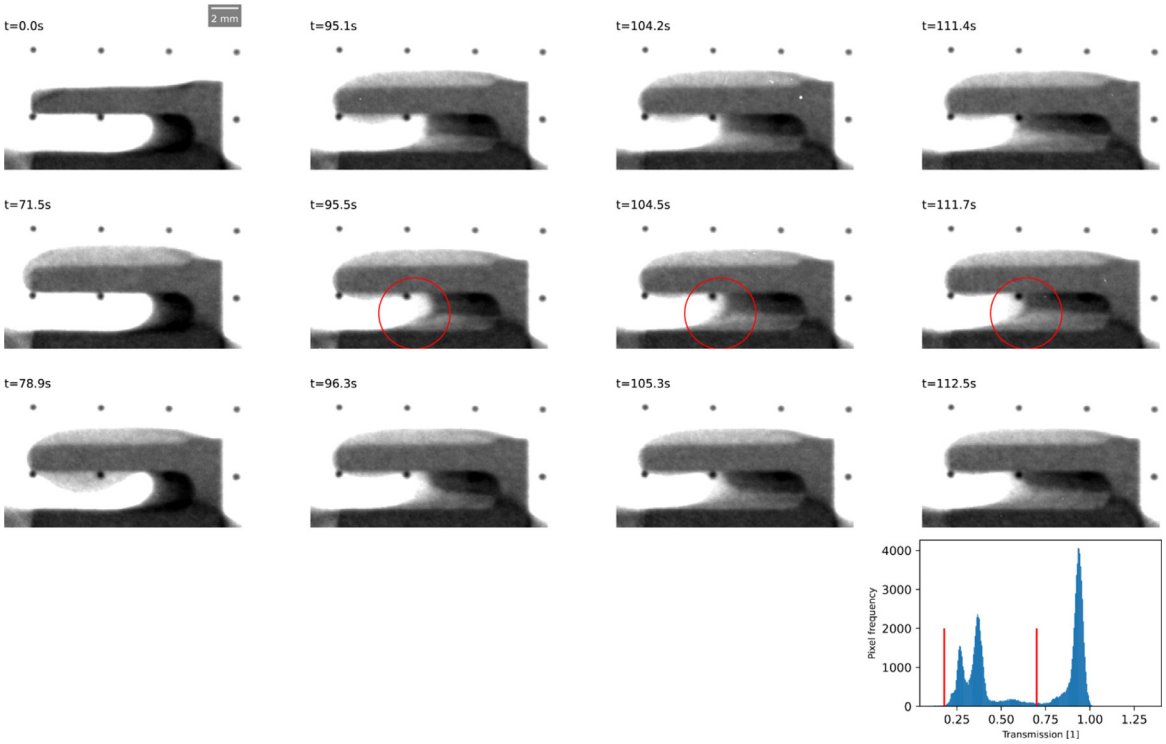


**Fig. 6.** Image sequence of absorbent impinging on a fin segment and flowing over the side while adhering to the fin underside, subsequently filling the lower set space between the fins with absorbent from right to left. The black dots are for orientation purpose only. The red vertical lines in the pixel frequency diagram indicate the gray level interval displayed (For interpretation of the references to color in this figure legend, the reader is referred to the web version of this article).

end of the fin. Accumulating droplets on the upper fin flow over the fin edge, suspending on the underside of the fin, seen at time 78.9 s, before bridging to the diluted absorbent and depositing under it. In the figure sequence starting at 95.1 s, three series of three images are displayed, showing conditions prior, during and post flow of concentrated absorbent from under the upper fin to the deposit between the fins. Separation of diluted to concentrated absorbent is clearly visible in all three sequences. In addition, it can be observed that as absorbent flows, there is a slight carry along of diluted absorbent, pointed to with the circles in the respective images. This downward movement of diluted absorbent is quickly counteracted and a clear separation of concentrated and diluted absorbent is restored as shown in the follow-up images.

### *3.4. Model spiral finned HMX*

A copper spiral finned tube is installed in the lab scale test bench. The spiral finned tube has an outer fin diameter of 21 mm, a length of 960 mm, a fin width of 4.5 mm and 2.8 mm fin spacing. The spiral finned HMX is tested under realistic absorption heat storage conditions at an evaporator HTF input temperature of 10 °C and flow of 700 ml/min and an absorber HTF input temperature of 25 °C with a flow of 100 ml/min. These conditions are considered to be realistic for the application in a home with floor heating and access to a ground source heat exchanger. The evaporator input temperature is the temperature available from the geothermal heat exchanger and the absorber input temperature is the return temperature from the building floor heating system.

## 4. Discussion

In the absorption storage heat pump, performance is measured by output temperature, power and volumetric energy density. All are bound by mass transport kinetics. In this visual study, measures are sought to optimize mass transport kinetics on the vertically installed spiral finned HMX by mixing, while keeping the single pass restriction. It is expected that by triggering absorbent mixing along the fin, concentration gradient in the film is reduced and rate of mass transport improved. A possible approach assessed is droplet formation and impingement by fin segmentation, cutting the fin so that a droplet forms at the end of a segment and falls onto the lower set fin segment. The results from the droplet on film impingement tests in Fig. 4, show that, the mixing effect is marginal, possibly due to lack of momentum of the impinging droplet and the high viscosity of NaOH solution, 47.7mPa s at 50wt% and 30 °C, relevant for the storage application. Especially from a film depth of 1 mm on, strict separation of diluted and concentrated absorbent is seen, with diluted absorbent rising to the top, slowing down absorption by increasing mass diffusion resistance. The fresh, concentrated absorbent droplets fall through and deposit under the diluted absorbent.

An alternative approach to increase absorption is found by absorbent suspension in a wire mesh. In this way, the exposure area of absorbent to absorbate is augmented. Again, rapid separation of diluted and concentrated absorbent is recognized. Contrary to the previous test, Fig. 5 shows that by suspending the absorbent droplet on a wire mesh, concentrated absorbent, on the bottom side, is directly and continuously exposed to the absorbate vapor. Practically no diffusion barrier to the absorbate evolves, since diluted absorbent rises to the top, re-exposing fresh concentrated absorbent on the bottom. It is esteemed that this process of diluted absorbent removal is even more effective than mixing, since absorbent with high concentration is continuously exposed to the absorbate vapor. In this case, it may be considered that mass transport by diffusion is even counterproductive since similar to mixing, it tends towards a mean concentration in the solution contacting the absorbate. In practice, substantial challenge in the design of a HMX, achieving stable suspension in HTF counter flow motion is

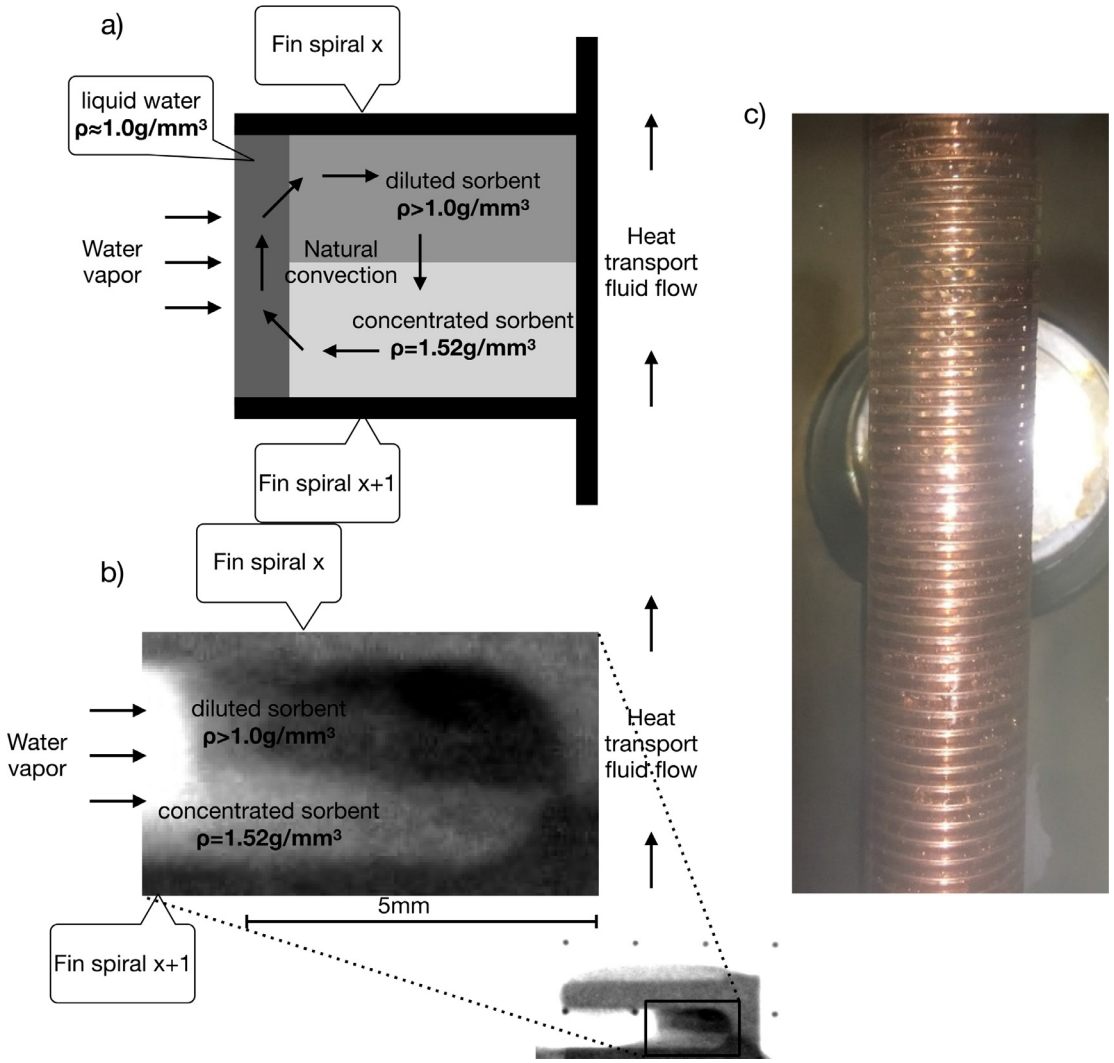


**Fig. 7.** a) Illustration of the water absorption and convection process in the fin space. The arrows indicate the vapor uptake, convection of diluted absorbent and exposing of concentrated absorbent to the absorption interface. b) Closeup of a fin segment neutron image, confirming the separation of concentrated absorbent (light gray) and diluted absorbent (dark gray), as well as the exposure of concentrated absorbent to the absorption interface. c) Image of the operating flooded spiral finned HMX.

anticipated. There is a strong tendency towards absorbent accumulation, building large droplets, that fall from their suspension [24].

A compromise between the favored conditions of droplet suspension and thin film flow on the spiral fin may be found in the fin segment evaluation. The images in Fig. 6 show that in the space between the upper and lower fin, alike concentration stratification occurs. This action exposes concentrated absorbent to the absorbate interface, where it rapidly absorbs vapor and rises to the underside of the upper fin releasing heat to the HTF in a continuous absorption and wash away process. This is also observed in Fig. 4b, where concentrated absorbent is exposed to the absorbate vapor due to the strong separation.

In all three varying analysis schemes, the separation of diluted to concentrated absorbent can be clearly detected. The source of this separation is proposed to be natural convection through change of concentration and temperature. Due to the good thermal conductivity of aqueous NaOH [25], thermal stratification is assumed minor in comparison to mass based effects [26], although both are equal in direction. An evaluation is possible based on the Rayleigh number $Ra = \Delta\rho g h^3 (D\eta)^{-1}$. Considering conditions in the heat storage application, with a density difference ($\Delta\rho$) of 525 kg $m^{-3}$, the difference between 50wt% aqueous NaOH and $H_2O$, the film height (h) of 2 mm, the mass diffusion coefficient (D) of $3.39 \times 10^{-11} m^2\ s^{-1}$, and the dynamic viscosity ($\eta$) of 0.048Pa s, a high Rayleigh number of $2.55 \times 10^7$ results, a clear indication for strong convection. The mass diffusion coefficient (D) is calculated according to the Stokes-Einstein equation $D = k_B \Theta (b\pi\eta r)^{-1}$ where $k_B$ is the Boltzmann constant ($1.380643E^{-23}$ J $K^{-1}$), $\Theta$ is the solution temperature of 303 K, b is a constant dependent on the molecule size relation, taken to be 6 in this case, $\eta$ is the dynamic viscosity of the absorbent taken to be 0.048Pa s, and r is the radius of the diffusing molecule, in this case water ($1.375 \times 10^{-10}$ m).

Fig. 7a illustrates the proposed process. A spiral finned tube is installed vertically as was followed in [8], whereby the spiral fin, perpendicular to the tube, is horizontal in a downwards moving helical spiral. The illustration (Fig. 7a) shows a segment cut, with the HTF on the right side and the fin spiral to the left. The fin is numbered as fin spiral x and $x + 1$, indicating a continuous single downward spiraling fin. The space between the spiraling fin is filled with absorbent having sideways vertical contact to the absorbate vapor. In this way, the absorbent is contained in a continuous stream in the spiraling fin. Issues with absorbent accumulation and fall through are prevented and the absorbent does not spill from the fin due to the sufficiently high liquid surface tension and mass-based stratification is actively employed to increase the rate of absorption. In the process, absorbate is condensed on

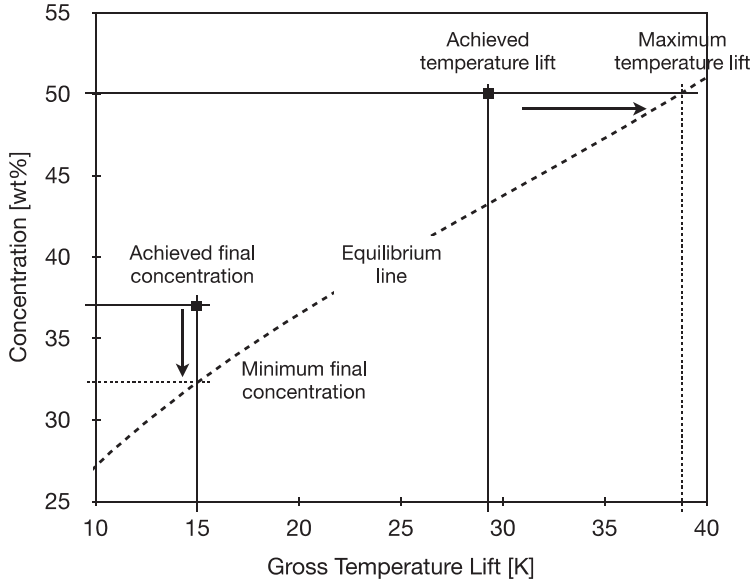


**Fig. 8.** Diagram showing the HMX performance in respect to the gross temperature lift and the concentration change, compared to the theoretical absorbate pressure, absorbent temperature and absorbent concentration equilibrium. The arrows indicate the potential improvement through increased buoyancy movement from design optimization.

the vertical absorbent surface, and the heat of condensation is released. Since the liquid absorbate, in this case water, is lighter than the absorbent, it rises to the underside of the higher set spiral, exposing fresh concentrated absorbent to the vertical contact surface. A continuous process of absorption, convection and fresh exposure results as illustrated in Fig. 7a. Fig. 7b shows a close up of a fin segment image (Fig. 6), emphasizing the detected process.

This concept is tested in the described lab scale single absorbent tube test setup [8]. The applied transported process, continuous supply of concentrated absorbent of 50wt% NaOH at a flow of 4 g/min to the top of the spiral finned tube, renders the system steady state operation with a continuous absorbent HTF output temperature of 37.5 °C. This is well sufficient for space heating; the European standard EN 14511 [27] requires 35 °C supply temperature for floor heating. The absorber HTF temperature lift is thus 12.5 K. On the evaporator, the HTF temperature drops from 10 °C input temperature to 8.2 °C output temperature, with a heat pump temperature lift, also referred to as gross temperature lift (GTL), between absorber output and evaporator output of 29.3 K. Compared to the theoretical maximum lift of 38 K under adiabatic open circuit conditions and considering the inclusion of temperature drop on the heat and mass exchanger, this achievement is favorable. The HMX has a power output of 84.2 W or an area specific power of 1.28 kW/m$^2$, referring to the active area of the absorber tube and not including the evaporator. The final discharged concentration is 37wt%. Under the testing conditions of 15 K difference between evaporator input (10 °C) and absorber input (25 °C) and adiabatic conditions, a theoretical concentration of 33wt% can be reached. Again, considering the running process, the achieved 37wt% is good. Based on the concentration difference, an energy density of 243 kWh/m$^3$ is calculated in respect to the volume of charged absorbent, the condition of greatest volume. This result is visualized in Fig. 8 in respect to the theoretical equilibrium between absorbate vapor pressure, absorbent temperature and absorbent concentration in a GTL vs. concentration diagram. The figure emphasizes the challenge encountered in the sorption storage heat pump, requiring both high temperature lift and low final concentration in a single pass discharge process, a challenge singular to the storage application, largely effecting the HMX design. The visualization in Fig. 8 provides a good basis for further performance evaluation of design changes for enhanced buoyancy movement both in respect to GTL and final concentration as indicated by the horizontal and vertical arrow.

## 5. Conclusion

In this study, strong convection triggered by concentration difference in the process of absorption is observed by neutron imaging experiments and associated with buoyancy changes. From these observation, a method for targeted engagement for liquid absorption heat storage is deduced. The designed flooded spiral finned tube HMX is expected to enable continuous exposure of concentrated absorbent to the absorbate in counterflow and with long exposure time. This eliminates the need for absorbent mixing along the spiral fin. Initial testing of such a spiral finned tube HMX have shown good performance in respect to the triple performance parameters; output temperature, power and energy density. Further work will now follow on the HMX design in order to evaluate best fin width and spacing to encourage exposure of concentrated absorbent through buoyancy movement and enable quantitative comparison.

## Declaration of Competing Interest

There are no conflicts of interest.

## Acknowledgement

This research work is financially supported by the Swiss Innovation Agency Innosuisse grant Nr. 1155002545 and is part of the Swiss Competence Centre for Energy Research SCCER HaE. Supplementary funding is received from the Swiss Federal Office of Energy SFOE grant Nr. SI/501605-01 in the frame of the IEA SHC Task 58/ECES Annex 33 participation. This work is based on experiments performed at the Swiss spallation neutron source SINQ, Paul Scherrer Institute, Villigen, Switzerland.

## Appendix: Challenge of absorption kinetics

The liquid absorption heat storage system comprises absorption heat pump and working pair storage tanks [28,29]. Absorbent

and absorbate are pumped from tank to heat pump and back and are stored in charged and discharged state. Operation distinguishes between charging (desorption and condensation) and discharging (evaporation and absorption), technically reducing heat pump components to a single HMX [30,31]. Owing to the interdependence of temperature lift and absorbent concentration, recirculation of absorbent solution for power enhancement is not applicable, requiring single pass discharge [8]. This is best fitted with absorbent and heat transfer fluid (HTF) counter-flow heat exchange, permitting maximum absorbent cooling (close to HTF input temperature), allowing for high absorbate uptake (equilibrium at low condensation temperature) and maximum HTF output temperature (close to absorbent maximum temperature) [32]. Absorbent flow, with exposure to absorbate vapor, is generally free, gravity based, while HTF flow is pumped [24,28]. Operation is performed under absorbate atmosphere [3,33] with good wetting, a practical design strain [24].

In the absorption heat storage, temperature lift and heat transport (power) are extended with energy capacity [3]. Ergo, a new scheme of operation manifests, centering on maximum absorbate uptake and heat release, requiring the advance towards absorbent equilibrium, an absorbent temperature, concentration and absorbate pressure dependent condition [34]. In absorption heat pumps, temperature lift and heat transport are enhanced through operation at high absorbent concentration with small concentration difference between absorption and desorption [35]. Measure of energy capacity impairs this approach for absorption heat storage, since large absorbate exchange is required between charged and discharged state to reach high energy density [36].

When looking into the process of absorption, in the phase transitions of pure substances, such as condensation of water vapor on liquid water, the gas-liquid interface is determining while in absorbent pools, diffusion is mass transfer rate limiting [37]. The laminar film model by Whitman is a common model taken to describe the absorption of a gas into a liquid [38], assuming a laminar gas–liquid interface layer as the predominant constriction to mass transfer of gas into the liquid phase [39]. In their studies, Tsai and Perez-Blanco conclude that surface-to-bulk mixing is required to increase the mass transport rates beyond molecular diffusion [40].

Absorbate mass flux to and from the absorbent surface is based on its vapor pressure, dependent on concentration gradient, limited by diffusion kinetics [41]. Acceleration is obtained through active (e.g. stirring) [42,43] or passive (e.g. impingement) [30] mixing, at best acquiring uniform temperature and concentration [44]. Typically, heat pumps exploit passive measures by absorbent impingement on a tube bundle at high absorbent flow rate [45]. Due to the low absorbent to absorbate exposure time, this design is not appropriate for absorption heat storage and suffers from low absorbate exchange in single pass [24].

In technical operation, kinetics of mass transport governs all three performance parameters, temperature lift, heat transport (power) and energy density. Under adiabatic condition, temperature lift from evaporator to absorber, is given by the absorbate vapor pressure on the absorbent, depending on the absorbent concentration [3,36]. In operation, surface concentration is reduced owing to mass transport rate limits from surface to bulk, limiting temperature lift [46]. Heat transport is coupled to both, absorbate transport rate and active (wetted) area. Energy density is dependent on the absorbate balance, charged to discharged state, bound by equilibrium conditions, limited by transport rate and exposure time [5].

Numerous studies have worked to adapt conventional absorption heat pump type heat and mass exchangers (HMX) for improved rate of absorption as required in the absorption heat storage. Mortazavi et al. addressed wetting issues for flat plate heat and mass exchanger operating with LiBr [6]. They proposed a finned structure to spread the absorbent on the falling film flat plate. Nevertheless, exposure time was low and single pass, a primary requirement, was not enabled. Michel et al. proposed a grooved plate falling film absorber, also not fitting to heat storage application [7]. Further research on novel flat plate falling film designs was reported by Hu et al. nevertheless they also needed to allow recirculation [47]. An extension of the tube bundle falling film HMX with M–W shaped corrugated mesh guides was reported by Chen et al. and Stehlík et al. propose finned surfaces on horizontal tubes, both again not reaching single pass [48,49].

In the development of absorption heat storage prototypes, the challenge has been encountered by many researches in the field, focusing on the common tube bundle falling film HMX design. N'Tsoukpoe et al. note a lack of mature absorption heat storage technology [50]. Zhang et al. adapt a lithium bromide absorption heat pump and fail to reach adequate energy density [51]. No heat gain is reached by N'Tsoukpoe et al. [28,30]. Le Pierrès et al. [52] reached only a low temperature lift and energy density. Daguenet-Frick et al. [24,53] also report insufficient temperature gain and energy density.

## References


[1] Editor(s): P. Le Goff, H. Matsuda, R. Rivero, Advances in chemical heat pumps and heat transformers, in: Takamoto Saito (Ed.), Heat Pumps, Pergamon, 1990, pp. 117–126.
[2] Editor(s): U. Jakob, 6 - Solar cooling technologies, in: Gerhard Stryi-Hipp (Ed.), Renewable Heating and Cooling, Woodhead Publishing, 2016, pp. 119–136.
[3] Editor(s): H.A. Zondag, Chapter 6 - Sorption heat storage, in: B. Sørensen (Ed.), Solar Energy Storage, Academic Press, 2015, pp. 135–154.
[4] B. Fumey, R. Weber, P. Gantenbein, X. Daguenet-Frick, I. Hughes, V. Dorer, Limitations imposed on energy density of sorption materials in seasonal thermal storage systems, Energy Procedia Volume 70 (2015) 203–208.
[5] B. Fumey, L. Baldini, A. Borgschulte, Water transport in aqueous sodium hydroxide films for liquid sorption heat storage, Energy Technol. 8 (2020) 2000187 https://doi.org/, doi:10.1002/ente.202000187.
[6] M. Mortazavi, R.N. Isfahani, S. Bigham, S. Moghaddam, Absorption characteristics of falling film LiBr (lithium bromide) solution over a finned structure, Energy 87 (2015) 270–278.
[7] B. Michel, N. Le Pierrès, B. Stutz, Performances of grooved plates falling film absorber, Energy 138 (2017) 103–117.
[8] B. Fumey, R. Weber, L. Baldini, Liquid sorption heat storage – a proof of concept based on lab measurements with a novel spiral fined heat and mass exchanger design, Appl. Energy 200 (2017) 215–225.
[9] A. Borgschulte, R. Delmelle, R.B. Duarte, A. Heel, P. Boillatc, E. Lehmann, Water distribution in a sorption enhanced methanation reactor by time resolved neutron imaging, PCCP 18 (2016) 17217–17223.
[10] A.P. Kaestner, S. Hartmann, G. Kühne, G. Frei, C. Grünzweig, L. Josic, F. Schmid, E.H. Lehmann, The ICON beamline – a facility for cold neutron imaging at SINQ, Nucl. Instrum. Methods Phys. Res. Sec. A 659 (1) (2011) 387–393.
[11] P. Trtik, J. Hovind, C. Grünzweig, A. Bollhalder, V. Thominet, C. David, A. Kaestner, E.H.E.H. Lehmann, Improving the spatial resolution of neutron imaging at paul scherrer institut – the neutron microscope project, Phys. Procedia 69 (2015) 169–176, doi:10.1016/j.phpro.2015.07.024.
[12] J. Banhart, Advanced Tomographic Methods in Materials Research and Engineering, Oxford University Press, Oxford, UK, 2008.
[13] L. Dobrzynski, K. Blinowski, Neutrons and Solid State Physics, Prentice Hall, 1994.
[14] A.H. Foderaro, in: The Elements of Neutron Interaction Theory, MIT Press, Cambridge, 1971, p. xiv.
[15] K. Sköld, D.L. Price, Neutron Scattering, Academic Press, Orlando, 1986.
[16] E.H. Lehmann, P. Vontobel, N. Kardjilov, Hydrogen distribution measurements by neutrons, Appl. Radiat. Isot. Volume 61 (Issue 4) (2004) 503–509.
[17] P. Trtik, M. Morgano, R. Bentz, E. Lehmann, 100Hz neutron radiography at the BOA beamline using a parabolic focussing guide, Methods X 3 (2016) 535–541.
[18] N. Kardjilov, M. Dawson, A. Hilger, I. Manke, M. Strobl, D. Penumadu, F.H. Kim, F. Garcia-Moreno, J. Banhart, A highly adaptive detector system for high resolution neutron imaging, Nucl. Instrum. Methods Phys. Res. Sec. A 651 (1) (2011) 95–99.
[19] G. Frei, E.H. Lehmann, D. Mannes, P. Boillat, The neutron micro-tomography setup at PSI and its use for research purposes and engineering applications, Nucl. Instrum. Methods Phys. Res. Sect. A 605 (1–2) (2009) 111–114.
[20] E.H. Lehmann, G. Frei, G. Kühne, P. Boillat, The micro-setup for neutron imaging: a major step forward to improve the spatial resolution, Nucl. Instrum. Methods Phys. Res. Sec. A 576 (2–3) (2007) 389–396.
[21] A.S. Tremsin, J.B. McPhate, J.V. Vallerga, O.H.W. Siegmund, J.S. Hull, W.B. Feller, E. Lehmann, High-resolution neutron radiography with microchannel plates:

proof-of-principle experiments at PSI, Nucl. Instrum. Methods Phys. Res. Sec. A 605 (1–2) (2009) 103–106.
[22] A.S. Tremsin, J.B. McPhate, J.V. Vallerga, O.H.W. Siegmund, J.S. Hull, W.B. Feller, E. Lehmann, Detection efficiency, spatial and timing resolution of thermal and cold neutron counting MCP detectors, Nucl. Instrum. Methods Phys. Res. Sec. A 604 (1–2) (2009) 140–143.
[23] B. Schillinger, H. Abele, J. Brunner, G. Frei, R. Gähler, A. Gildemeister, A. Hillenbach, E. Lehmann, P. Vontobel, Detection systems for short-time stroboscopic neutron imaging and measurements on a rotating engine, Nucl. Instrum. Methods Phys. Res. Sect. A 542 (1–3) (2005) 142–147.
[24] X. Daguenet-Frick, P. Gantenbein, J. Müller, B. Fumey, R. Weber, Seasonal thermo- chemical energy storage: comparison of the experimental results with the modelling of the falling film tube bundle heat and mass exchanger unit, Renew. Energy 110 (2017) 162–173.
[25] A.A. Alexandrov, The equations for thermophysical properties of aqueous solutions of sodium hydroxide, 14th International Conference on the Properties of Water and Steam in Kyoto, 2005.
[26] B. Fumey, L. Baldini, A. Borgschulte, Water transport in aqueous sodium hydroxide films for liquid sorption heat storage, Energy Technol. 8 (2020) 2000187 https://doi.org/, doi:10.1002/ente.202000187.
[27] EN 14511. Air conditioners, liquid chilling packages and heat pumps with electrically driven compressors for space heating and cooling—part 2: test conditions
[28] K.E. N'Tsoukpoe, N. Le Pierrès, L Luo, Experimentation of a LiBr-$H_2O$ absorption process for long term solar thermal storage, Energy Proced. 30 (2012) 331–341.
[29] B. Fumey, R. Weber, P. Gantenbein, X. Daguenet-Frick, T. Williamson, V. Dorer, Development of a closed sorption heat storage prototype, Energy Procedia 46 (2014) 134–141.
[30] K.E. N'Tsoukpoe, N. Le Pierrès, L. Luo, Experimentation of a LiBr–$H_2O$ absorption process for long-term solar thermal storage: prototype design and first results, Energy 53 (2013) 179–198.
[31] X. Daguenet-Frick, P. Gantenbein, E. Frank, B. Fumey, R. Weber, T. Williamson, Reaction zone development for an aqueous sodium hydroxide seasonal thermal energy storage, Energy Procedia 57 (2014) 2426–2435.
[32] B. Fumey, R. Weber, L. Baldini, Sorption based long-term thermal energy storage – process classification and analysis of performance limitations: a review, Renewable Sustainable Energy Rev. 111 (2019) 57–74.
[33] X. Zhang, M. Li, W. Shi, B. Wang, X. Li, Experimental investigation on charging and discharging performance of absorption thermal energy storage system, Energy Convers Manag. 85 (2014) 425–434.
[34] Editor J.R. Fair, D.E. Steinmeyer, W.R. Penney, S.M. Crocker, Gas absorption and gas-liquid system design, in: RH Perry (Ed.), Perry's Chemical Engineers' Handbook McGraw-Hill, 2007. eighth ed..
[35] Editor(s) Z.Y. Xu, R.Z. Wang, 11 - Solar-powered absorption cooling systems, in: R.Z. Wang, T.S. Ge (Eds.), Advances in Solar Heating and Cooling, Woodhead Publishing, 2016, pp. 251–298.
[36] H. Liu, K.E.K.E. N'Tsoukpoe, N. Le Pierres, L. Luo, Evaluation of a seasonal storage system of solar energy for house heating using different absorption couples, Energy Convers. Manage. 52 (6) (2011) 2427–2436.
[37] E.Y.E.Y. Gatapova, I.A.I.A. Graur, O.A.O.A. Kabov, V.M.V.M. Aniskin, M.A.M.A. Filipenko, F. Sharipov, L. Tadrist, The temperature jump at water – air interface during evaporation, Int. J. Heat Mass Transf. 104 (2017) 800–812.
[38] W.G.W.G. Whitman, The two-film theory of gas absorption, Chem. Metall. Eng. 29 (1923) 146–148.
[39] P.V. Danckwerts, A.M. Kennedy, Kinetics of liquid-film process in gas absorption. Part I: models of the absorption process, Chem. Eng. Res. Des. 75 (Supplement) (1997) S101–S104 https://doi.org/, doi:10.1016/S0263-8762(97)80007-X.
[40] B.B. Tsai, H. Perez-Blanco, Limits of mass transfer enhancement in lithium bromide-water absorbers by active techniques, Int J Heat Mass Transf 41 (15) (1998) 2409–2416 https://doi.org/, doi:10.1016/S0017-9310(97)00287-1.
[41] P. Danckwerts, The absorption of gases in liquids, Pure Appl. Chem. 10 (4) (1965) 625–642.
[42] Y. Jiru, D.A. Eimer, A study of mass transfer kinetics of carbon dioxide in (monoethanolamine + water) by stirred cell, Energy Procedia 37 (2013) 2180–2187.
[43] P.D. Vaidya, E.Y. Kenig, Gas–liquid reaction kinetics: a review of determination methods, Chem. Eng. Commun. 194 (2007) 1543–1565.
[44] Perry's Chemical Engineers' Handbook, Eighth Edition
[45] A. Behfar, Z. Shen, J. Lau, Y. Yu, Heat and mass transfer enhancement potential on falling film absorbers for water-LiBr mixtures via a literature review (RP-1462), HVAC&R Res. 20 (5) (2014) 570–580.
[46] Crank J. The Mathematics of Diffusion. ISBN 9780198534112
[47] T. Hu, X. Xie, Y. Jiang, Design and experimental study of a plate-type falling–film generator for a LiBr/$H_2O$ absorption heat pump, Int. J. Refrig. 74 (2017) 304–312.
[48] Y. Chen, R. Cao, J. Wu, Z. Yi, G. Ji, Alternate heat and mass transfer absorption performances on staggered tube bundle with M–W corrugated mesh guider inserts, Int. J. Refrig. 66 (2016) 10–20.
[49] P. Stehlík, Z. Jegla, B. Kilkovský, Possibilities of intensifying heat transfer through finned surfaces in heat exchangers for high temperature applications, Appl Therm Eng 70 (2) (2014) 1283–1287.
[50] K.E. N'Tsoukpoe, H. Liu, N. Le Pierrès, L. Luo, A review on long-term sorption solar energy storage, Renew. Sustain. Energy Rev. 13 (9) (2009) 2385–2396.
[51] X. Zhang, M. Li, W. Shi, B. Wang, X. Li, Experimental investigation on charging and discharging performance of absorption thermal energy storage system, Energy Convers Manag. 85 (2014) 425–434.
[52] N. Le Pierrès, F. Huaylla, B. Stutz, J. Perraud, Long-term solar heat storage process by absorption with the KCOOH/$H_2O$ couple: experimental investigation, Energy 141 (2017) 1313–1323.
[53] X. Daguenet-Frick, M. Dudita, L. Omlin, P. Gantenbein, Seasonal thermal energy storage with aqueous sodium hydroxide – development and measurements on the heat and mass exchangers, Energy Proced. 155 (2018) 286–294.